Authors' accepted manuscript.
The final publication is available at ELSEVIER: Sensors and Actuators B: Chemical, via:
http://dx.doi.org/10.1016/j.snb.2013.06.053

Probabilistic Gas Quantification with MOX Sensors in Open Sampling Systems - A Gaussian Process Approach

Javier G. Monroy, Achim Lilienthal, Jose Luis Blanco, Javier Gonzalez-Jimenez and Marco Trincavelli[12]

Abstract

Gas quantification based on the response of an array of metal oxide (MOX) gas sensors in an open sampling system is a complex problem due to the highly dynamic characteristic of turbulent airflow and the slow dynamics of the MOX sensors. However, many gas related applications require to determine the gas concentration the sensors are being exposed to. Due to the chaotic nature that dominates gas dispersal, in most cases it is desirable to provide, together with an estimate of the mean concentration, an estimate of the uncertainty of the prediction. This work presents a probabilistic approach for gas quantification with an array of MOX gas sensors based on Gaussian Processes, estimating for every measurement of the sensors a posterior distribution of the concentration, from which confidence intervals can be obtained. The proposed approach has been tested with an experimental setup where an array of MOX sensors and a Photo Ionization Detector (PID), used to obtain ground truth concentration, are placed downwind with respect to the gas source. Our approach has been implemented and compared with standard gas quantification methods, demonstrating the advantages when estimating gas concentrations.

Keywords: Gas Quantification, Open Sampling System, MOX sensors,

1. Introduction

Gas sensing applications often require continuous and direct exposition of gas sensors to the environment to be analyzed. Some examples are the on-line monitoring of landfill sites and industrial processes [1], pollution monitoring [2, 3], exploration of hazardous areas [4] or de-mining.

This configuration, to which we refer as Open Sampling System (OSS), is the preferred solution when limitations in dimension, payload or energy consumption do not allow the adoption of a sampling system where the sensors are hosted in a chamber with controlled airflow, temperature and humidity. In addition, the dynamic response of the sensor when directly exposed to the environment contains useful information about the nature of a gas plume, information which may be inaccessible for sensors hosted inside a chamber and affected by a controlled airflow. The information gained from the dynamic response may be crucial for solving tasks like gas source localization [5, 6, 7] or gas distribution mapping [8, 9].

The most common gas sensing technology for OSS applications is metal oxide (MOX) gas sensors. MOX sensors are conductometric sensors, which means that the conductance of the oxide changes when a gas interacts with the sensing surface. The most prominent reasons for the popularity of MOX sensors are their wide commercial availability, low price, and a higher sensitivity to the compounds of interest in comparison to most other gas sensing technologies. However, this technology presents among other drawbacks, an important lack of selectivity, that it does not provide true concentration read-

ings, suffers from long and short term drift and is rather slow [10], especially when recovering to the baseline [11] (i.e. the steady output value given by a gas sensor when exposed to clean air).

The problem addressed in this paper is the estimation of gas concentration from the readings of an array of MOX sensors deployed in an OSS. In other words, the problem can be formalized as finding a function that maps the readings of N gas sensors together with any other extra parameters (like temperature and humidity) to a posterior distribution over concentrations.

Concentration estimation is a crucial step for realistic gas sensing applications since legal requirements and regulations are expressed in terms of absolute gas concentration, toxicity levels, etc. For example, it would be of little utility for many applications if we could detect a gas leak in an industrial scenario but we were unable to *quantify* the amount of leaked gas: should an alarm be issued for workers to abandon the area, or is localization of the source and subsequent notification to the maintenance unit enough to handle the problem?

Gas quantification using an array of MOX sensors in an OSS is indeed an important problem. Surprisingly, only few attempts to approach this problem can be found in the literature. Most of the previous works dealing with OSS do not estimate the concentration of the gas but work directly with the sensor signal (conductance readings in case of MOX gas sensors). However, in contrast to gas quantification with sensors within a sensing chamber (where controlled conditions can be imposed), gas quantification with sensors in OSS implies additional complications due to the many sources of uncertainty. The most relevant source of uncertainty is the exposition of the sensors to the

turbulent airflow that brings the chemical compound in contact with the sensors. As a consequence, given the slow dynamics of MOX gas sensors and the rapid fluctuations in concentration due to turbulent airflow, the sensors never reach a steady state but continuously fluctuate [12]. In other words, the true concentration causes a range of different response levels due to the effects introduced by the slow transient in the response and the quick fluctuations due to turbulence. This range corresponds to a wide variance of the posterior distribution over concentration.

In order to deal with the identified difficulties for MOX sensors in OSS, in this paper we present an approach for concentration estimation that, instead of trying to find a deterministic function for mapping directly the sensors readings to concentration values, calculates instead a posterior distribution over concentrations c at time t given the measurements of N sensors $\mathbf{r_t} = (r_1(t), r_2(t) \dots r_N(t))$ at times $\mathbf{t} = (t_1, \dots, t_k)$. That is, we search a probability density function:

$$p\left(c(t)|\mathbf{r_{t_1}}, \dots, \mathbf{r_{t_k}}\right) \tag{1}$$

where k is the number of past sensor readings considered for the prediction.

A key advantage of having a full posterior distribution instead of a single prediction value of the gas concentration is that probabilistic inference is possible, which uses the notion of uncertainty about the actual concentration. Tasks like chemical detection, gas source localization, gas distribution mapping, and odour trail tracking are common tasks for working in OSS. For this kind of systems it is acceptable to have only an approximate estimate of the concentration if there is also an indication of the corresponding confidence.

This is exactly what the method proposed in this work provides.

In this paper we propose to estimate the posterior in Eq. (1) using a Gaussian Process (GP) model [13]. Gaussian Processes provide principled supervised machine learning methods which, given a set of samples (i.e. pairs of sensor readings and their corresponding concentration), can estimate the posterior joint probability of the process. The ground truth concentration values are obtained using a Photo Ionization Detector (PID) placed in the vicinity of the MOX sensor array. Unlike MOX gas sensors, if the chemical compound is known, the PID provides true concentration measurements. Moreover the response dynamics of a PID is much quicker compared to MOX sensors, and, therefore the latter can follow the true concentration changes more closely.

However, PIDs are of little help when the gas to quantify is unknown since they provide a concentration value corresponding to the mixture of all present gases with an ionization energy below what their ionization unit delivers. Furthermore, they are also expensive, and it is therefore also of economical interest to be able to estimate gas concentrations accurately with inexpensive MOX sensors, considering in particular also applications in a sensor network.

We analyze gas quantification using either a single sensor or the whole sensor array, extending our previous work [14] where only a single sensor was employed. In the latter context we additionally investigate how Automatic Relevance Determination (ARD) [15] [16] can be used to identify which sensors in the array contribute most to the estimate of the concentration posterior distribution. Finally, we analyze to which extent considering

past sensor readings can improve the accuracy of probabilistic calibration.

The structure of this article is as follows. After a discussion of related work in Section 2, we introduce in Section 3 the basics of Gaussian Process regression for gas quantification, giving special attention to learning a GP from the data. Then, Section 4 presents the experimental setup and finally, comparative results under different configurations of the GP are presented in Section 5, followed by conclusions and suggestions for future work in Section 6.

2. Related Work

Estimation of gas concentration from raw readings of MOX-based gas sensors has been a major research topic for many years. Research has been traditionally focused on setups where such sensors are enclosed inside a chamber, where environmental conditions, gas exposure times and concentrations are known and controlled. This setup allows the measurement of steady state values, which are used as input to a regressor. Under such controlled conditions, the relation between sensor conductance (Ω^{-1}) and gas concentration (ppm) is usually modelled as an exponential [17]:

$$g_i \equiv \frac{1}{r_i} = A_i \cdot c^{\alpha_i} \tag{2}$$

where g_i is the conductance of sensor i within the array (inverse of sensor resistance r_i), c is the gas concentration, and A_i and α_i are the parameters of the exponential model to be estimated during an initial training process.

For concentration estimation with an array of MOX sensors, multivariate linear regression methods like Principal Component Regression (PCR) and

Partial Least Squares Regression (PLSR) have been proposed [18, 19, 20]. The main motivation behind the use of these two methods is the strong correlation of the response of different MOX sensors. This allows both, PCR and PLSR, to reduce the dimensionality of the input space before fitting a regression function, thus reducing the possibility of *curse of dimensionality* related issues. Alternatively, non-linear estimation methods like Artificial Neural Networks (ANN) [21, 22] or kernel algorithms like Support Vector Regression (SVR) [23, 24] have also been proposed.

It is worth noting that some authors consider the transient information for MOX sensor calibration. In [25], a multi-exponential model is used to describe the sensor dynamics and to predict the steady state value of the sensors which is then mapped to a concentration based on the initial values of the transient state.

These existing calibration approaches rely on steady state measurements of the sensor. Thus, they are not immediately applicable to OSS because steady state values are almost never reached [12], due to turbulent advection, which dominates gas transport in the target environments.

The work in [26] addressed calibration of an e-nose for urban pollution monitoring. Measurements collected over a long period of time are averaged out and therefore the dynamic information in the sensor response is discarded. The focus of our work is instead on applications where sensors are deployed in a highly dynamic environment, where they are exposed to intermittent patches of gas.

Most of the work in mobile robot olfaction avoids calibration issues and use instead the conductance readings of the sensors as an approximate mea-

sure of the gas concentration. An exception is [27], where Ishida et al. propose to use steady state calibration to obtain a rough approximation of gas concentration with an OSS.

All the methods mentioned ignore the uncertainty in the calibration, which is present in an OSS with MOX sensors due to the turbulence-dominated gas transport mechanisms, the sensor dynamics and environmental factors such as temperature or humidity (temperature and humidity are not addressed in this work, however). It is desirable to quantify the uncertainty together with the concentration estimate. The GP-based method proposed in this paper generates an estimate of the uncertainty (as a variance), which can be used, for example, to calculate confidence intervals for the predictions.

3. The algorithm for estimation of gas concentration.

This section details our proposal for the concentration estimation in MOX-OSS. Initially, two signal preprocessing methods and their influence on the posterior distribution estimation are described. Next, Gaussian Process regression for the particular case of gas quantification with an array of sensors is summarized, and how Automatic Relevance Determination can be used to select the model parameters. Finally, two different loss functions are proposed for evaluating the results, allowing a comparison between the various proposed configurations.

3.1. Signal Preprocessing

In the first step, the raw sensor resistance readings $r_i(t)$ are divided by the baseline of the sensor at $t = 0$, that is, $r_i(0)$. This transformation in Eq. (3),

known as relative baseline manipulation [28],is applied for drift compensation and dynamic range enhancement:

$$\tilde{\mathbf{r}}_\mathbf{t} = [\tilde{r}_i(t)]_{i=1}^N, \tilde{r}_i(t) = \frac{r_i(t)}{r_i(0)} \tag{3}$$

Next, GP regression is used to predict the gas concentration $c(t)$ from the values $\tilde{\mathbf{r}}_\mathbf{t}$. However, considering the commonly assumed exponential relation between sensor resistance and the concentration, see Eq. (2), we will also investigate applying a logarithmic transformation and perform regression between $\log(\tilde{\mathbf{r}}_\mathbf{t})$ and $\log(c(t))$.

In summary, we will compare two regression problems:

$$c(t) = f_1(\tilde{\mathbf{r}}_\mathbf{t}) \tag{4}$$

$$\log c(t) = f_2(\log \tilde{\mathbf{r}}_\mathbf{t}) \tag{5}$$

3.2. Gaussian Process Regression for Gas Concentration Estimation

In the general case, the process of inferring the relationship $f : \mathbf{r}_\mathbf{t} \longmapsto c(t)$ between the response of an array of sensors and the gas concentration using a training dataset $\mathbf{D} = \{(\mathbf{r}_{t_j}, c(t_j)|j = 1, ..., n\}$ is a supervised machine learning problem. Among the numerous available options, GPs provide a powerful non-parametric tool for Bayesian inference and learning [13]. GPs can be seen as a generalization of the Gaussian probability distribution to distributions over functions. That is, they perform inference directly in the space of functions, starting with a prior distribution over all possible functions and subsequently learning the target function from data samples. Defining a prior over functions corresponds to making assumptions about the characteristics

of the function f, as otherwise any function which is consistent with the training data will be equally valid and therefore the learning problem would be ill-defined.

A GP is completely specified by its mean and covariance functions, $m(\mathbf{r_t})$ and $k(\mathbf{r_t}, \mathbf{r_{t'}})$ respectively:

$$\begin{aligned} m(\mathbf{r_t}) &= \mathbb{E}\left[f(\mathbf{r_t})\right], && (6) \\ k(\mathbf{r_t}, \mathbf{r_{t'}}) &= cov\left(f(\mathbf{r_t}), f(\mathbf{r_{t'}})\right) && (7) \\ &= \mathbb{E}\left[(f(\mathbf{r_t}) - m(\mathbf{r_t}))(f(\mathbf{r_{t'}}) - m(\mathbf{r_{t'}}))\right]. && (8) \end{aligned}$$

we denote the GP as:

$$f\left(\mathbf{r_t}\right) \sim \mathcal{GP}\left(m(\mathbf{r_t}), k(\mathbf{r_t}, \mathbf{r_{t'}})\right). \quad (9)$$

To account for noise in the sensor it is assumed that the observed concentration values $c(t)$ are corrupted with an additive i.i.d. Gaussian noise with zero mean and variance σ_n^2, that is:

$$\begin{aligned} c(t) &= f(\mathbf{r_t}) + \varepsilon, && (10) \\ \varepsilon &\sim \mathcal{N}(0, \sigma_n^2). \end{aligned}$$

It is important to notice that we did not assess experimentally whether the noise is i.i.d. with Gaussian distribution. We rather make this assumption to obtain a closed form solution, and validate the resulting predictions with real sensor data.

In our case of study we consider GPs with zero mean and the commonly used squared exponential (SE) covariance function, that is:

$$m(\mathbf{r_t}) = 0, \tag{11}$$

$$k(\mathbf{r_t}, \mathbf{r_{t'}}) = \sigma_f^2 \exp\left(-\frac{1}{2}\frac{\| \mathbf{r_t} - \mathbf{r_{t'}} \|^2}{\ell^2}\right), \tag{12}$$

where σ_f^2 is the overall variance hyper-parameter and ℓ is the characteristic length scale. It is common but not necessary to consider GPs with zero mean. Note that the mean of the posterior process is not restricted to be zero. The choice of the SE covariance function leads to GP predictions that are *smooth* over the characteristic length scale. That is, if $\mathbf{r_t} \approx \mathbf{r_{t'}}$, then $k(\mathbf{r_t}, \mathbf{r_{t'}})$ approaches its maximum and $f(\mathbf{r_t})$ is strongly correlated with $f(\mathbf{r_{t'}})$. For large distances between $\mathbf{r_t}$ and $\mathbf{r_{t'}}$, $k(\mathbf{r_t}, \mathbf{r_{t'}})$ approaches 0. So, when predicting the concentration value for new data points, distant observations will have a negligible effect. The region of influence, depends on the scale parameter ℓ.

The regression model depends on the selection of the hyper-parameters, which are summarized in a vector $\boldsymbol{\theta} = (\ell^2, \sigma_f^2, \sigma_n^2)$. The optimal hyper-parameters are found by maximizing the marginal likelihood function $p\left(\mathbf{c}|\mathbf{R}, \boldsymbol{\theta}\right)$, where $\mathbf{c}$ is a vector of training concentration values, $\mathbf{R}$ is the matrix containing the measurements of the sensor array, and $\boldsymbol{\theta}$ are the hyper-parameters. As it is common practice, we minimize the corresponding negative log-likelihood to avoid numerical issues:

$$
\begin{aligned}
-\log\left(p(\mathbf{c}|\mathbf{R},\boldsymbol{\theta})\right) &= \frac{1}{2}\mathbf{c}^\top\mathbf{K}^{-1}\mathbf{c} + \frac{1}{2}\log|\mathbf{K}| + \frac{n}{2}\log 2\pi \qquad (13)\\
\text{where}\,\mathbf{K} &= k(\mathbf{r_t},\mathbf{r_{t'}}) + \sigma_n^2\mathbf{I}
\end{aligned}
$$

To find the minimum of Eq. (13) we use the scaled conjugate gradient method, which requires the calculation of the partial derivatives of the log marginal likelihood w.r.t. the hyper-parameters:

$$
\begin{aligned}
\frac{\partial}{\partial\theta_j}\log\left(p(\mathbf{c}|\mathbf{R},\boldsymbol{\theta})\right) &= \frac{1}{2}tr\left[\left(\boldsymbol{\alpha}\boldsymbol{\alpha}^\top - \mathbf{K}^{-1}\right)\frac{\partial\mathbf{K}}{\partial\theta_j}\right] \qquad (14)\\
\text{where}\,\boldsymbol{\alpha} &= \mathbf{K}^{-1}\mathbf{c}
\end{aligned}
$$

The complexity of this step is dominated by the matrix inversion $\mathbf{K}^{-1}$ in Eq. (14), which has a complexity $\mathcal{O}(n^3)$ with n being the number of training points. This represents one of the principal inconveniences of GP.

Learning the calibration GP corresponds to the selection of the hyper-parameters. The GP then allows to predict gas concentration values $\mathbf{c}_*$ and a corresponding variance for arbitrary sensor resistances $\mathbf{r}_*$.

The posterior distribution over functions (our prediction) is also a Gaussian, and it is given by:

$$
\begin{aligned}
\mathbf{c}_*|\mathbf{R},\mathbf{c},\mathbf{R}_* &\sim \mathcal{N}\left(\bar{\mathbf{c}}_*, cov(\mathbf{c}_*)\right), \text{where} \qquad (15)\\
\bar{\mathbf{c}}_* &\triangleq \mathbb{E}[\mathbf{c}_*|\mathbf{R},\mathbf{c},\mathbf{R}_*] = \mathbf{K}(\mathbf{R}_*,\mathbf{R})[\mathbf{K}(\mathbf{R},\mathbf{R}) + \sigma_n^2\mathbf{I}]^{-1}\mathbf{c}\\
cov(\mathbf{c}_*) &= \mathbf{K}(\mathbf{R}_*,\mathbf{R}_*) - \mathbf{K}(\mathbf{R}_*,\mathbf{R})[\mathbf{K}(\mathbf{R},\mathbf{R}) + \sigma_n^2\mathbf{I}]^{-1}\mathbf{K}(\mathbf{R},\mathbf{R}_*)
\end{aligned}
$$

and where $\mathbf{R} = \{\mathbf{r}_1 ... \mathbf{r}_n\}$ is the $n \times N$ matrix of the n training samples of dimensionality N, $\mathbf{R}_*$ the matrix for the testing inputs, $\mathbf{K}(\cdot,\cdot)$ refers to the

matrix with the entries given by the covariance function $k(\cdot,\cdot)$ and $\mathbf{c}$ the vector of the observed concentrations c_i.

Note that the predictive distribution is based on a mean value $\bar{\mathbf{c}}_*$ (our best estimate for $\mathbf{c}_*$), which is a linear combination of the observed values $\mathbf{c}$, and a variance value $cov(\mathbf{c}_*)$ which denotes the uncertainty in our estimation, and does not depend on the observed targets but only on the inputs.

3.3. Automatic Relevance Determination

Automatic Relevance Determination (ARD) is a method based on Bayesian interference for pruning large feature sets with the aim to obtain a sparse explanatory subset. Making use of this powerful tool we can consider different configurations of the input space of higher dimensionality, and then allow ARD to select the most relevant features, which avoids overfitting due to high input dimensionality. In order to introduce ARD Eq. (12) can be rewritten as:

$$k(\mathbf{r_t}, \mathbf{r_{t'}}) = \sigma_f^2 \exp\left(-\frac{1}{2}(\mathbf{r_t} - \mathbf{r_{t'}})^\top \mathbf{M}(\mathbf{r_t} - \mathbf{r_{t'}})\right), \tag{16}$$

where $\mathbf{M}$ denotes the diagonal weight matrix $\mathbf{M} = \ell^{-2}\mathbf{I}$.

We have seen how maximizing the log marginal likelihood can be used to determine the value of the hyper-parameters. By incorporating a separate hyper-parameter ℓ_i for each input variable [13], i.e. for each sensor in the array, we modify $\mathbf{M}$ to be:

$$\mathbf{M} = diag\left([\ell_1^{-2}, \ell_2^{-2}, \ldots, \ell_n^{-2}]\right) \tag{17}$$

where $\boldsymbol{\ell} = [\ell_1, \ell_2, \ldots, \ell_n]$ is a vector of positive values, corresponding to the

length-scale of each input variable. This is in contrast to a *global* hyper-parameter ℓ for all input variables.

Since the inverse of the length-scale determines how relevant an input is, the extension (17) enables to identify the importance of each different input– if the length-scale has a very large value, the covariance will become almost independent of that input, effectively ignoring its values during the inference.

ARD is performed during the training phase of the GP, specifically during the selection of the covariance function hyper-parameters. When the inputs related to a sensor are discarded by ARD, the corresponding sensors can be excluded from the array. In this work, ARD has been applied for two different configurations of the input space: (i) when the whole sensor array is considered at one instant of time in the inference process and (ii) when additional features from previous time steps of the sensor response are considered to account for the dynamics of the signal.

3.4. Evaluation of the Predictions

To compare different configurations of the GP based calibration proposed in this paper, among themselves, and with other methods previously proposed in the literature, two performance measures are proposed:

Root Mean Squared Error (RMSE): The RMSE is calculated as the difference between the ground-truth concentration (obtained with the readings from a PID sensor) and the expected value of the predictive distribution obtained from Eq. (15).

$$RMSE = \sqrt{\frac{1}{n}\sum_{i=1}^{n}(c_i - \bar{c}_{*i})^2} \tag{18}$$

Notice that the RMSE takes only into account the predictive mean, while it ignores its uncertainty. However, this indicator allows to compare the predictions of the proposed GP calibration approach with other regression methods, like Partial Least Squares Regression (PLSR) or Support Vector Regression (SVR), which do not provide any estimation of the prediction uncertainty.

Negative Log Predictive Density (NLPD): The NLPD is a standard criterion to evaluate probabilistic models (see Eq. (19)).

$$NLPD = -\frac{1}{n}\sum_{i=1}^{n}\log(p(c_i|\mathbf{r_i})) \tag{19}$$

It is worth noting that the NLPD considers the whole posterior distribution and not only its expected value. In general, more negative NLPD values indicate better predictions with a small uncertainty.

Considering the two preprocessing methods proposed in Section 3.1, two different NLPD formulas arise. In the first case (linear preprocessing - Eq. (4)), the posterior distribution of the concentration is a normal distribution, while in the second case, (logarithmic preprocessing - Eq. (5)), the posterior distribution of the concentration is a log-normal distribution. Therefore the NLPD is calculated for the two cases respectively:

$$NLPD_{normal} = \frac{\log(2\pi)}{2} + \frac{1}{2N}\sum_{i=1}^{n}\left[\log(\sigma^2(c_i)) + \frac{(c_i - \mu(c_i))^2}{\sigma^2(c_i)}\right] \tag{20}$$

Authors' accepted manuscript.
The final publication is available at ELSEVIER: Sensors and Actuators B: Chemical, via:
http://dx.doi.org/10.1016/j.snb.2013.06.053

$$NLPD_{log-normal} = \frac{\log(2\pi)}{2} + \frac{1}{2N}\sum_{i=1}^{n}\left[\log(c_i^2\sigma^2(c_i)) + \frac{(\log(c_i) - \mu(c_i))^2}{\sigma^2(c_i)}\right]$$

where c_i is the ground truth gas concentration, $\sigma(c_i)$ is the predictive standard deviation, and $\mu(c_i)$ the predictive mean.

4. Experimental Setup

The experiments are carried out in a 4.85 m $\times$ 3.42 m $\times$ 2 m room with an induced artificial airflow of approximately 0.1 m/s. The airflow is created using two arrays of six standard microprocessor cooling fans. The gas source is an odour blender (olfactory display), a device described in [29] that can mix up to 13 gas components from arbitrary recipes using rapidly switching solenoid valves. The odour blender samples from the headspace of the compounds, which are kept in liquid phase. This odour blender enables rapid switching of compound and concentration. The odour blender uses headspace sampling and therefore does not intensify evaporation, contrary to an odour bubbler [30]. The outlet of the olfactory blender is placed on the floor, 0.5 m upwind with respect to an array of 11 MOX gas sensors and a PID[3]. The airflow at the outlet of the odour blender is set to 1 l/min. Figure 1 displays the configuration of the experiments. The sensors included in the array are listed in Table 1. The sensors are sampled at 4 Hz. The PID is placed next to the array of MOX sensors in order to obtain calibrated measurements in the proximity of the active area of the MOX sensors. This is important since, due to diffusion and advection, the estimation of the gas

[3]PID model ppbRAE2000 from RAESystem with a 10.6 eV UV lamp.

concentration at the sensors would be very complicated if only the intensity of the gas source would be available. The position of the MOX sensors and the PID has been carefully chosen in order to ensure that the sensors are exposed to a very similar gas concentration. This can be verified calculating the Pearson's coefficient to estimate the linear correlation among the response of the sensors. From the results reported in Table 2 it is clear that the response of the MOX sensors and the PID are highly correlated and therefore it can be inferred that the sensors are exposed to very similar concentration profiles. Due to the faster sensor dynamics, the correlation of the PID response with the response of the MOX sensors is in general slightly lower than the correlation between the response of two MOX sensors. The compound selected for these experiments is ethanol, which is heavier than air and, consequently, forms plumes at ground level.

[Figure 1 about here.]

[Table 1 about here.]

[Table 2 about here.]

In order to create a dataset that represents a variety of scenarios, four different odour emitting profiles have been used (see Figure 2). For all the profiles the gas source does not emit gas for two minutes (this is equivalent to releasing no gas) and the signal of the sensors during this period is assumed as the baseline. Also, at the end of all the experiments the source emits clean air for 2 minutes. Overall, the dataset includes a total of 18 experiments, 3 for the deterministic emission strategies and 9 for the randomized emission strategy.

[Figure 2 about here.]

5. Results

In this section we present and compare the gas sensor calibration results obtained with the two preprocessing methods (linear & logarithmic).

We further compare three different sets of input variables. First, we consider the sensors independently. Second, we compare to the case where the whole array is considered as the input to the inference process. Third, we discuss the effect of including the dynamics of MOX sensors by using delayed sensor samples as part of the input space.

For the evaluation we used cross-validation, selecting the folds at the experiment level and not at the sample level. This means that if samples from an experiment have been used during the training procedure, no sample from that experiment was used for calculating the performance measures. In this way an optimistic bias in the results due to evaluation with samples collected in the same trial, i.e. under exactly equal environmental conditions, is avoided. All the experiments have been carried out in the time span of one week and therefore effects due to long term drift are not considered in this work. Furthermore, due to the computational complexity of the training algorithm of the GP (which is dominated by the inversion of the kernel matrix, to be performed at every step of the maximization of the marginal likelihood) a subset of 1000 points from the experiments considered for the training set, was randomly selected for training the GP.

We compare the proposed calibration method with Partial Least Squares Regression (PLSR) and Support Vector Machine Regression (SVR) for all

input configurations. Since both methods only provide an estimate of the gas concentration without information about its uncertainty, only the RMSE can be used as a performance indicator for comparison. Please note that PLSR and SVR have been widely used in classical sensor calibration in controlled environments. Nevertheless, in this work we apply PLSR and SVR to data obtained with an OSS in a very dynamic environment.

5.1. Gas Quantification Using a Single Sensor

A typical sensor response in an OSS is depicted in Figure 3. The PID measurements displayed in Figure 3(b) show the fast fluctuations around an average value to which the MOX sensors are exposed when the output of the gas source is steady. These fluctuations are caused by the turbulent airflow and are the reason why the MOX gas sensors do not reach a steady state.

[Figure 3 about here.]

For the case of single gas sensor input, i.e. a univariate function $f : r_i \longmapsto c$, it is possible to plot the relation between sensor resistance and gas concentrations obtained in the experiments (see Figure 4). Notice how the distribution of training points (represented by blue dots) corresponds to uncertainty about the measured concentration.

[Figure 4 about here.]

The predictive variance is not necessarily constant across the whole input space, but it depends on the density and dispersion of the training points. If many training points are available in a certain region, then the predictive variance goes down to the global estimate of the signal variance (given by

the hyper-parameter σ_f). On the other hand, when few or no training points are available in a region, the predictive variance in that region increases indicating less reliable estimates.

In our case, since we used a uniform distribution to sample the input space for selecting the training points, the posterior variance turns out to be almost constant over the input space (see Figure 4(a)). It can be seen in Figure 4 that a constant variance does not describe the true signal variance adequately. When the inference is carried out after applying the logarithmic transformation to the sensor resistance and gas concentration, however, the predictive variance represents more accurately the variance in the training points, see Figure 4(b). This shows that the process generating the data is indeed not Gaussian and is therefore modelled better by a Log-Normal (non-Gaussian) process. Nevertheless, we can efficiently obtain this non-Gaussian Process by applying a non-linear transformation to the data and then performing Gaussian Process regression.

The estimated gas concentrations for three different gas emitting strategies are displayed in Figure 5 and Figure 6 for the linear and logarithmic preprocessing respectively. A notable difference exists between the predictive uncertainty in the two cases. In Figure 7 and Figure 8 the NLPD and RMSE are plotted for each sensor in the array using a box-plot format. When calibrating using the linear relation we obtain, in average over all the sensors, a RMSE of $35.15 \pm 10.32 ppm$, and a NLPD of 5.16 ± 0.71, while for logarithmic preprocessing the achieved average RMSE is $31.17 \pm 6.27 ppm$ and the NLPD is 4.27 ± 0.18. The results after applying the log transformation in Eq. (5) are better according to both performance measures.

[Figure 5 about here.]

[Figure 6 about here.]

[Figure 7 about here.]

[Figure 8 about here.]

From the results in Figures 7 and 8 we can also see that the sensors *TGS-2611* and *MiCS-5121* perform best for the specific target gas (ethanol).

Table 3 summarizes the comparison of the proposed GP calibration with PLSR and SVR. For the same input, the RMSE, averaged over all sensors is $33.77 \pm 5.77 ppm$ for the PLSR approach and $30.94 \pm 6.78 ppm$ for the SVR approach. The PLSR approach performs slightly worse than SVR, and SVR is on par with the GP approach considering only the RMSE. A possible explanation for this result is that PLSR is a linear method while both SVR and GP are non-linear and use an SE (RBF) kernel.

[Table 3 about here.]

5.2. Gas Quantification Using a Sensor Array

In OSS applications where the goal is discriminating among several different odours [31], an array of MOX sensors is usually employed instead of a single sensor. For this reason, we investigate whether also gas quantification benefits from using the whole sensor array. In order to do this we apply the GP calibration method with an input space of dimension $d = 11$, and apply ARD (see Section 3.3) to automatically select the most relevant inputs, that is, the most relevant gas sensors in the array.

Table 4 summarizes the mean and the $\pm 1\sigma$ confidence interval of the normalized length scale hyper-parameter (l) for the different sensors in the array, after ARD has been computed for the 13 folds used in the cross-validation. As explained in Section 3, large values of the length scale corresponds to less relevant sources of information.

[Table 4 about here.]

Our results show that sensors which perform well in the case of single sensor calibration are in most cases also relevant for array calibration. An exception is the sensor *TGS-2602*, which did not perform well individually, but was found to provide valuable information when considering the whole array (*TGS-2602* is the second most relevant sensor according to ARD but was ranked last in its individual GP calibration performance, see Table 3). Figures 9 and 10 show gas concentration estimates for three different scenarios when considering the readings of the eleven sensors at once.

[Figure 9 about here.]

[Figure 10 about here.]

In general, the gas concentration estimation obtained using the whole array of sensors outperforms the estimation based on a single sensor. Linear preprocessing provides an average RMSE of $16.44 \pm 3.38 ppm$ and a NLPD of 4.22 ± 0.20, while for the logarithmic preprocessing the results are slightly better: RMSE of $15.97 \pm 2.77 ppm$, NLPD of 3.59 ± 0.76.

In comparison, PLSR applied to the same input achieves a RMSE of $17.55 \pm 2.42 ppm$ which, is slightly worse than the GPs calibration, as in the

single sensor case (Section 5.1). SVR achieves a RMSE of $16.20 \pm 2.50 ppm$, very similar to the results obtained with the GP approach but without providing the additional information about the uncertainty in the prediction.

The uncertainty estimate is particularly meaningful when the posterior distribution is modelled as a Log-Normal distribution, rather than with a Gaussian distribution. High uncertainty estimates (which can be identified in the left column of Figure 10 and Figure 8 in the case of predictions performed with a single sensor) correspond to an increased mean and variance of the RMSE (observable in the right column of Figures 10 and 8). This describes the observed fluctuations in the signal well and thus provides a reliable confidence measure for concentration predictions.

Our results also lead to the conclusion that it is recommendable to start using the whole sensor array and select the most relevant sensors with ARD. This allows for better concentration estimate.

5.3. Taking into account the dynamics of MOX gas sensors

The signals from MOX gas sensors in an OSS are strongly influenced by the sensor dynamics. The uncertainty about concentration estimates is due to the chaotic nature of gas transport in combination with the sensor dynamics, i.e. the non-negligible response and recovery times of the MOX sensors. In this section we propose two different extensions so that the proposed GP calibration can automatically account for the dynamics of MOX sensors. Both methods augment the input signal: the first method ("Memory") by additionally considering delayed samples of every sensor in the input variables (in a so called tapped delay line). The second method ("Derivatives") accounts for the dynamics of each sensor by considering the derivatives of the

signal in addition to the signal itself. Figure 11 depicts the gas quantification results when considering both alternatives. For the first case ("Memory"), the x-axis $k = 0 \dots 5$ represents the number of additional delayed samples for each training point, while in the second case it represents the maximum order of derivatives taken into account as additional inputs to the inference process.

[Figure 11 about here.]

The first conclusion from these results is that our GP calibration was not able to infer the dynamics of MOX sensors from delayed samples of the sensor signals, and thus, the calibration results do not improve when increasing k. Furthermore, and possibly due to the increase in the input dimensionality, the results tend to get worse for high values of k, probably due to curse of dimensionality. On the other hand, the "Derivatives" approach yields slightly positive results. The improvement is mainly observable in the RMSE where mean as well as the confidence intervals decrease when increasing k.

6. Conclusions and Future Work

In this paper we proposed a new approach for gas concentration estimation using an array of MOX gas sensors in a Open Sampling System (OSS). Despite its importance, this topic has been largely neglected. We addressed the problem in a probabilistic manner and used Gaussian Processes to estimate a posterior distribution over the gas concentration given the response from an array of MOX sensors. This has the advantage of enabling not only

predictions of the expected gas concentration but also predictions of the uncertainty of this estimate. This advantage is particularly relevant for OSS applications where typically many sources of uncertainty exist.

In the first part of this work, we focussed on gas quantification using a single MOX sensor, and then turned to gas quantification using a sensor array. We found a clearly improved prediction quality with a sensor array compared to using a single sensor. Given the high correlation among different MOX sensors, we used ARD to exclude sensors that are not relevant for estimating the posterior distribution. This proves useful in keeping the dimensionality of the input space low.

We also analysed two data preprocessing strategies, one that performs GP regression directly with the sensor response and ground truth gas concentrations, and a second one that performs GP regression on the logarithms of sensor response and ground truth concentrations. Logarithmic preprocessing has proven advantageous both for the estimation of the expected gas concentration and for uncertainty prediction.

Finally, we studied approaches to mitigate the effect of the slow dynamics of MOX sensors by taking into account past sensor readings in the GP regression. Neither using additional inputs from previous time steps, nor adding the signal derivatives, produced a significant improvement over the concentration estimation algorithm that considers only the current sensors readings.

Future works will include exploring sparse Gaussian Processes like the Relevance Vector Machine (RVM) or Informative Vector Machine (IVM) to improve over the currently random selection of training points, which is a

major bottleneck for GP regression. Another interesting aspect to study is the generation of confidence intervals on the prediction and in particular how the Bayesian approach we propose here compares with frequentist approaches like Conformal Prediction (CP). Finally, another aspect to investigate is the use of kernels for time series like the Autoregressive (AR) or Dynamic Time Warping (DTW) kernel to study if they can efficiently model the dynamics of MOX sensors, and therefore produce even more accurate gas concentration estimates.

Acknowledgements

The authors would like to thank Hiroshi Ishida, Yuichiro Fukazawa and Yuta Wada for the support in the data collection phase.

This work has been partly supported by the Regional Government of Andalucía and the European Union (FEDER) under research contract P08-TEP-4016.

References

[1] V. Hernandez Bennetts, A. Lilienthal, M. Trincavelli, Creating true gas concentration maps in presence of multiple heterogeneous gas sources, 2012, pp. 554–557.

[2] M. Trincavelli, M. Reggente, S. Coradeschi, H. Ishida, A. Loutfi, A. J. Lilienthal, Towards environmental monitoring with mobile robots, in: Proceedings of the IEEE/RSJ International Conference on Intelligent Robots and Systems (IROS), 2008, pp. 2210 – 2215.

[3] M. Reggente, A. Mondini, G. Ferri, B. Mazzolai, A. Manzi, M. Gabelletti, P. Dario, A. J. Lilienthal, The dustbot system: Using mobile robots to monitor pollution in pedestrian area, Chemical Engineering Transactions 23 (2010) 273–278. doi:10.3303/CET1023046.

[4] P. P. Neumann, S. Asadi, A. J. Lilienthal, M. Bartholmai, J. H. Schiller, Autonomous gas-sensitive microdrone: Wind vector estimation and gas distribution mapping, Robotics Automation Magazine, IEEE 19 (1) (2012) 50–61. doi:10.1109/MRA.2012.2184671.

[5] G. Kowadlo, R. A. Russell, Robot odor localization: A taxonomy and survey, The International Journal of Robotics Research 27 (8) (2008) 869–894.

[6] A. J. Lilienthal, A. Loutfi, T. Duckett, Airborne chemical sensing with mobile robots, Sensors 6 (2006) 1616–1678.

[7] H. Ishida, T. Nakamoto, T. Moriizumi, T. Kikas, J. Janata, Plume-tracking robots: A new application of chemical sensors, The Biological Bulletin 200 (2) (2001) 222–226.

[8] J.-L. Blanco, J. G. Monroy, J. González-Jiménez, A. Lilienthal, A kalman filter based approach to probabilistic gas distribution mapping, in: 28th Symposium On Applied Computing (SAC), 2013.

[9] A. J. Lilienthal, M. Reggente, M. Trincavelli, J. L. Blanco, J. Gonzalez, A statistical approach to gas distribution modelling with mobile robots the kernel dm+v algorithm, in: Proceedings of the IEEE/RSJ Interna-

tional Conference on Intelligent Robots and Systems (IROS), 2009, pp. 570–576.

[10] A. J. Lilienthal, T. Duckett, A stereo electronic nose for a mobile inspection robot, in: Proceedings of the IEEE International Workshop on Robotic Sensing (ROSE), Örebro, Sweden, 2003.

[11] J. Gonzalez-Jimenez, J. G. Monroy, J. L. Blanco, The multi-chamber electronic nose - an improved olfaction sensor for mobile robotics, Sensors 11 (6) (2011) 6145–6164. doi:10.3390/s110606145.

[12] M. Trincavelli, Gas discrimination for mobile robots, Künstliche Intelligenz 25 (4) (2011) 351 – 354.

[13] C. Rasmussen, C. Williams, Gaussian processes for machine learning, Adaptive computation and machine learning, MIT Press, 2006.

[14] J. Monroy, A. Lilienthal, J. Blanco, J. Gonzalez-Jimenez, M. Trincavelli, Calibration of mox gas sensors in open sampling systems based on gaussian processes, in: Sensors, 2012 IEEE, 2012, pp. 1–4. doi:10.1109/ICSENS.2012.6411464.

[15] R. Neal, Bayesian learning for neural networks, Lecture notes in statistics, Springer, 1996.

[16] D. J. C. MacKay, Bayesian methods for back-propagation networks, Models of neural networks 3, Springer, 1994, pp. 211–254.

[17] K. Ihokura, J. Watson, The stannic oxide gas sensor: principles and applications, CRC Press, 1994.

[18] P. J. Gemperline, J. R. Long, V. G. Gregoriou, Nonlinear multivariate calibration using principal components regression and artificial neural networks, Analytical Chemistry 63 (20) (1991) 2313–2323. doi:10.1021/ac00020a022.

[19] H. Sundgren, F. Winquist, I. Lukkari, I. Lundstrom, Artificial neural networks and gas sensor arrays: Quantification of individual components in a gas mixture, Measurement Science and Technology 2 (5) (1991) 464–469.

[20] K. Domansk, D. L. Baldwin, J. W. Grate, T. B. Hall, J. Li, M. Josowicz, J. Janata, Development and calibration of field-effect transistor-based sensor array for measurement of hydrogen and ammonia gas mixtures in humid air, Analytical Chemistry 70 (3) (1998) 473–481. doi:10.1021/ac970427x.

[21] L. Hadjiiski, P. Geladi, P. Hopke, A comparison of modeling nonlinear systems with artificial neural networks and partial least squares, Chemometrics and Intelligent Laboratory Systems 49 (1) (1999) 91–103.

[22] M. Blanco, J. Coello, H. Iturriaga, S. Maspoch, J. Pags, Calibration in non-linear near infrared reflectance spectroscopy: A comparison of several methods, Analytica Chimica Acta 384 (2) (1999) 207–214.

[23] A. Shmilovici, G. Bakir, S. Marco, A. Perera, Finding the best calibration points for a gas sensor array with support vector regression, in: Intelligent Systems, 2004. Proceedings. 2004 2nd International IEEE Conference, Vol. 1, 2004, pp. 174 – 177 Vol.1. doi:10.1109/IS.2004.1344660.

[24] R. P. Cogdill, P. Dardenne, Least-squares support vector machines for chemometrics: An introduction and evaluation, Journal of Near Infrared Spectroscopy 12 (2) (2004) 93–100.

[25] C. D. Natale, S. Marco, F. Davide, A. D'Amico, Sensor-array calibration time reduction by dynamic modelling, Sensors and Actuators B: Chemical 25 (1-3) (1995) 578 – 583, proceedings of the Fifth International Meeting on Chemical Sensors. doi:10.1016/0925-4005(95)85126-7.

[26] S. D. Vito, E. Massera, M. Piga, L. Martinotto, G. D. Francia, On field calibration of an electronic nose for benzene estimation in an urban pollution monitoring scenario, Sensors and Actuators B: Chemical 129 (2) (2008) 750 – 757. doi:10.1016/j.snb.2007.09.060.

[27] H. Ishida, T. Nakamoto, T. Moriizumi, Remote sensing of gas/odor source location and concentration distribution using mobile system, Sensors and Actuators B: Chemical 49 (1-2) (1998) 52 – 57. doi:10.1016/S0925-4005(98)00036-7.

[28] T. Pearce, Handbook of machine olfaction: electronic nose technology, Wiley-VCH, 2003.

[29] T. Nakamoto, K. Yoshikawa, Movie with scents generated by olfactory display using solenoid valves, IEICE Trans. Fundam. Electron. Commun. Comput. Sci. E89-A (11) (2006) 3327–3332. doi:10.1093/ietfec/e89-a.11.3327.

[30] R. Russell, Odour Detection by Mobile Robots, World Scientific Publishing Co, London, UK, 1999.

[31] M. Trincavelli, S. Coradeschi, A. Loutfi, Online classification of gases for environmental exploration, in: Proceedings of the IEEE/RSJ International Conference on Intelligent Robots and Systems (IROS), 2009, pp. 3311 – 3316.

Javier G.Monroy received his MSc degree (2007) in Electrical Engineering from the University of Málaga, Spain. Currently, he is a graduate student at the Dept. of System Engineering and Automation, University of Málaga. During spring 2011 he visited the Center for Applied Autonomous Sensor Systems, Örebro University, Sweden, as a guest researcher. His research interests include autonomous mobile robots and artificial olfaction.

Achim Lilienthal is professor at AASS, Örebro University, Sweden, where he is leading the Mobile Robotics and Olfaction Lab. His main research interests are mobile robot olfaction, rich 3D perception, robot vision, and safe navigation for autonomous transport robots. Achim Lilienthal obtained his Ph.D. in computer science from Tübingen University, Germany and his M.Sc. and B.Sc. in Physics from the University of Konstanz, Germany. The Ph.D. thesis addresses gas distribution mapping and gas source localisation with a mobile robot. The M.Sc. thesis is concerned with an investigation of the structure of $(C_{60})_n^+$ clusters using gas phase ion chromatography.

Jose Luis Blanco was born in Linares, Spain, in 1981. He received the European PhD and the M.S. degree in Electrical Engineering from the University of Málaga, Málaga, Spain in 2009 and 2005, respectively. Currently, he teaches as a Lecturer at the University of Almería, Spain. He is the author or coauthor of about 20 journal and conference papers. His current research interests include robot autonomous navigation, world modeling, and

computer vision.

Javier González-Jimenez received the B.S. degree in Electrical Engineering from the University of Seville in 1987. He joined the Department of "Ingeniera de Sistemas y Automática" at the University of Málaga in 1988 and received the Ph.D. from this University in 1993. In 1990-1991 he was at the Field Robotics Center, Robotics Institute, Carnegie Mellon University (USA) working on mobile robots as part of his PhD. Since 1996 he has been leading Spanish and European projects on mobile robotics and perception. Currently, he is a professor at the University of Málaga and head of the Machine Perception and Intelligent Robotics (MAPIR) group. His research interest includes mobile robot navigation, olfactory robotics and computer vision. In these fields he has published three books and more than 100 papers.

Marco Trincavelli received both his BSc degree (2003) and his MSc degree (2006) in Computer Engineering from the Politecnico di Milano, Milan, Italy. He additionally received a MSc degree in Electrical Engineering and Computer Science from the Lund Tekniska Högskola, Lund, Sweden, in 2006. In 2007-2010 he has been a graduate student at the Center for Applied Autonomous Sensor Systems, Örebro University, Örebro, Sweden. During autumn 2009 he visited the Tokyo University of Agriculture and Technology as a guest researcher. In autumn 2010 he spent another period as a guest researcher at the BioCircuits Institute at the University of California, San Diego. His research interests include machine learning and artificial olfaction with particular focus on mobile robotics applications.

List of Figures

Authors' accepted manuscript.
The final publication is available at ELSEVIER: Sensors and Actuators B: Chemical, via:
http://dx.doi.org/10.1016/j.snb.2013.06.053

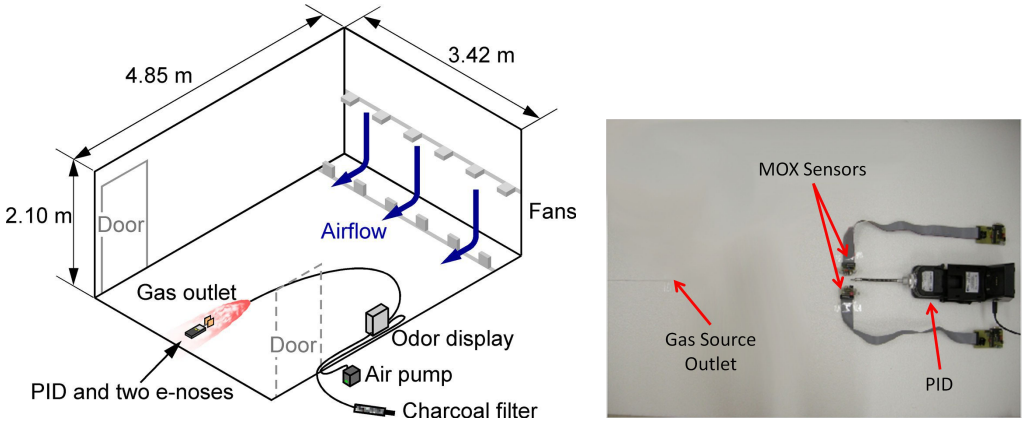

(a) (b)

Figure 1: Sketch of the experimental setup (a), and detailed picture of the MOX sensors and the PID used to sample the volatiles (b).

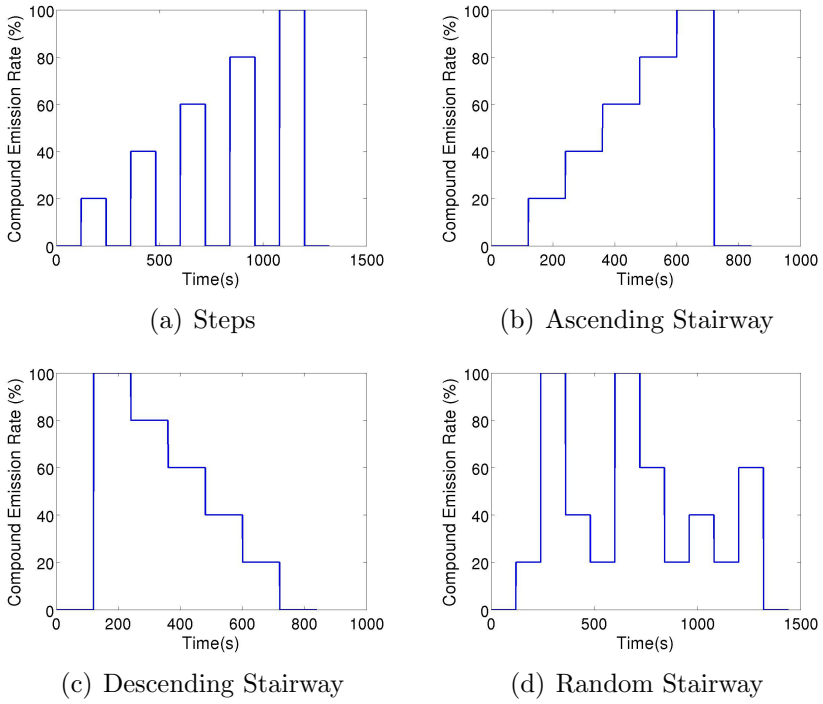

(a) Steps (b) Ascending Stairway

(c) Descending Stairway (d) Random Stairway

Figure 2: Gas source emission strategies. For the randomized strategy (d), one exemplary instance is displayed.

Authors' accepted manuscript.
The final publication is available at ELSEVIER: Sensors and Actuators B: Chemical, via:
http://dx.doi.org/10.1016/j.snb.2013.06.053

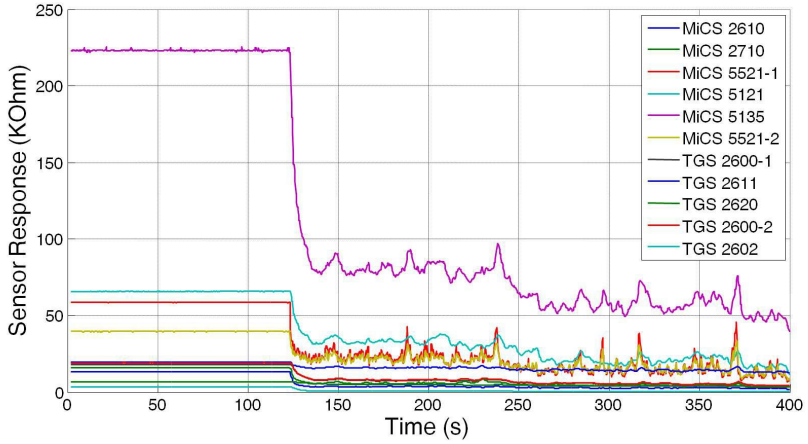

(a)

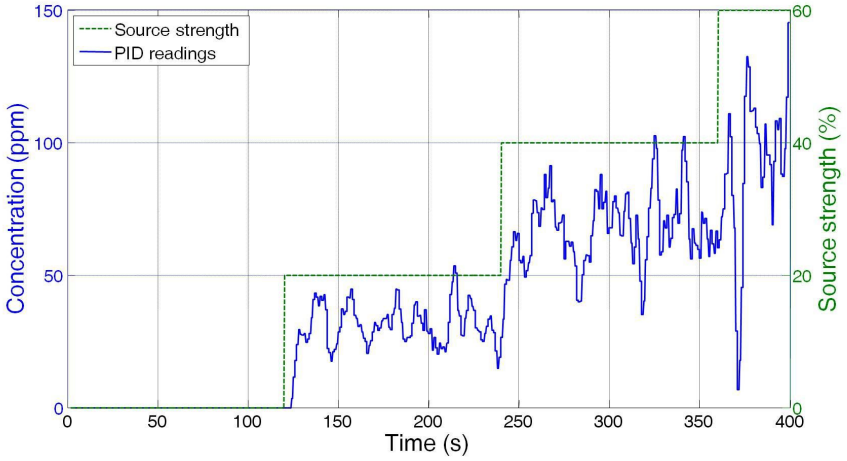

(b)

Figure 3: Instantaneous sensor response (a) and PID measurements (b) for a standard open sampling system experiment.

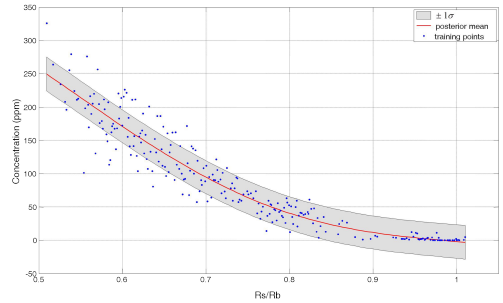

(a)

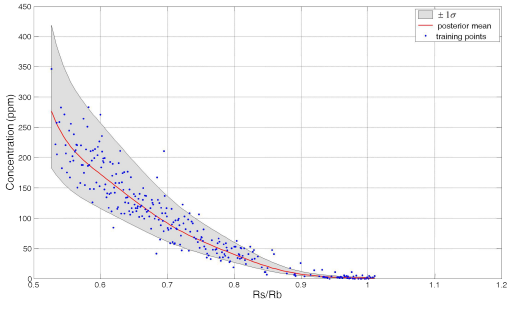

(b)

Figure 4: Examples of the learned regression functions for the case where a single sensor (here *TGS-2611*) is considered. Blue dots represent the training data. The solid red line is the mean of the posterior, and its variance is visualized by the $\pm 1\sigma$ confidence interval. (a) A typical calibration function learned when using linear pre-processing, Eq. (4). (b) Calibration after applying a logarithmic transformation not only to the input data, Eq. (5).

Authors' accepted manuscript.
The final publication is available at ELSEVIER: Sensors and Actuators B: Chemical, via:
http://dx.doi.org/10.1016/j.snb.2013.06.053

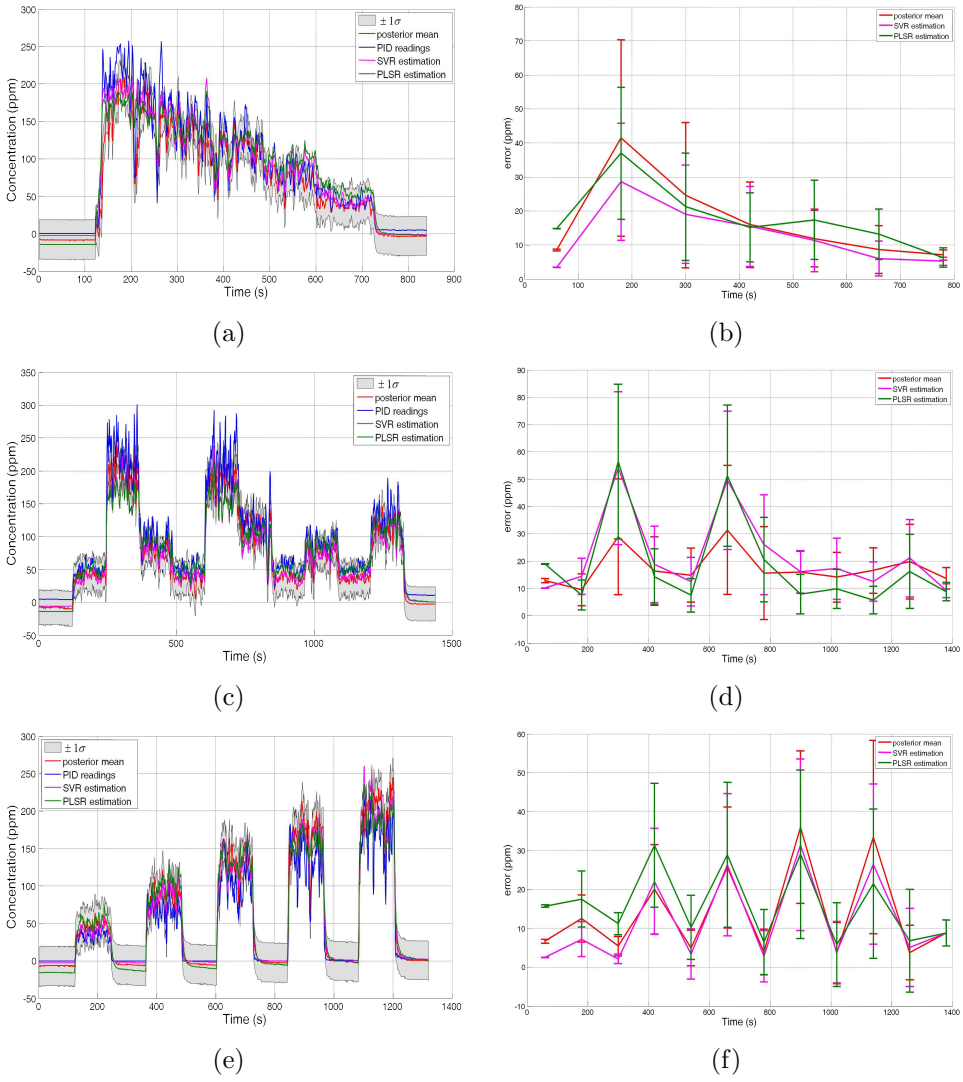

Figure 5: Estimation of the gas concentration for three different gas emitting strategies (rows), obtained from sensor *TGS-2611* with linear pre-processing $c = f(\tilde{r}(t))$, and the proposed GP calibration. The left column shows the ground truth (blue) together with the GP calibration estimate (the red line is the posterior mean and the shaded grey region represents $\pm 1\sigma$ confidence interval), the PLSR (green line), and the SVR estimate (magenta line). The right column shows for each scenario the error between the different estimates and ground truth (in the case of GPs only the mean value is taken into account).

Authors' accepted manuscript.
The final publication is available at ELSEVIER: Sensors and Actuators B: Chemical, via:
http://dx.doi.org/10.1016/j.snb.2013.06.053

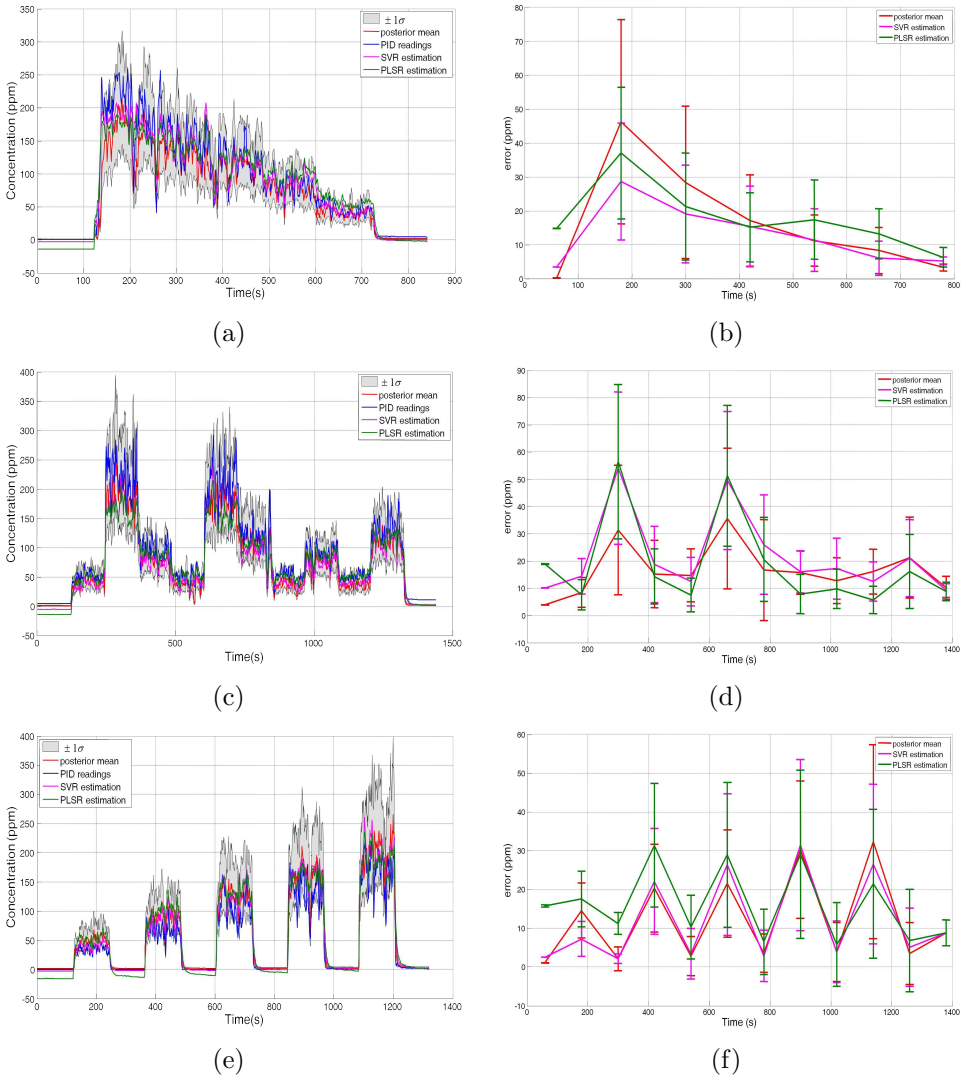

Figure 6: The predictions of the same experiment as in Figure 5, but after training on log-transformed inputs: $\log(c) = f(\log(\tilde{r}_i(t)))$.

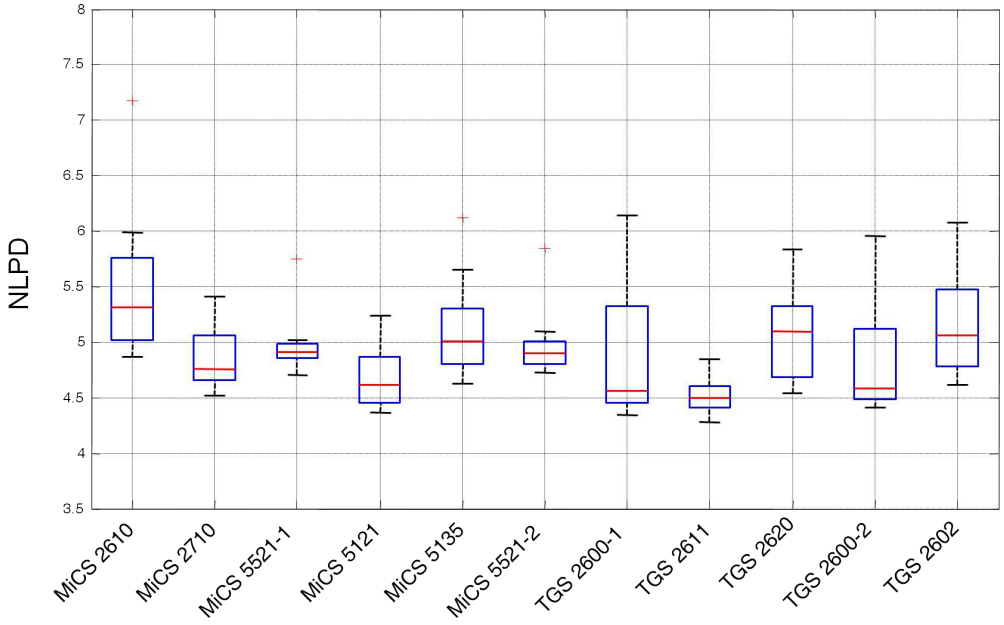

(a)

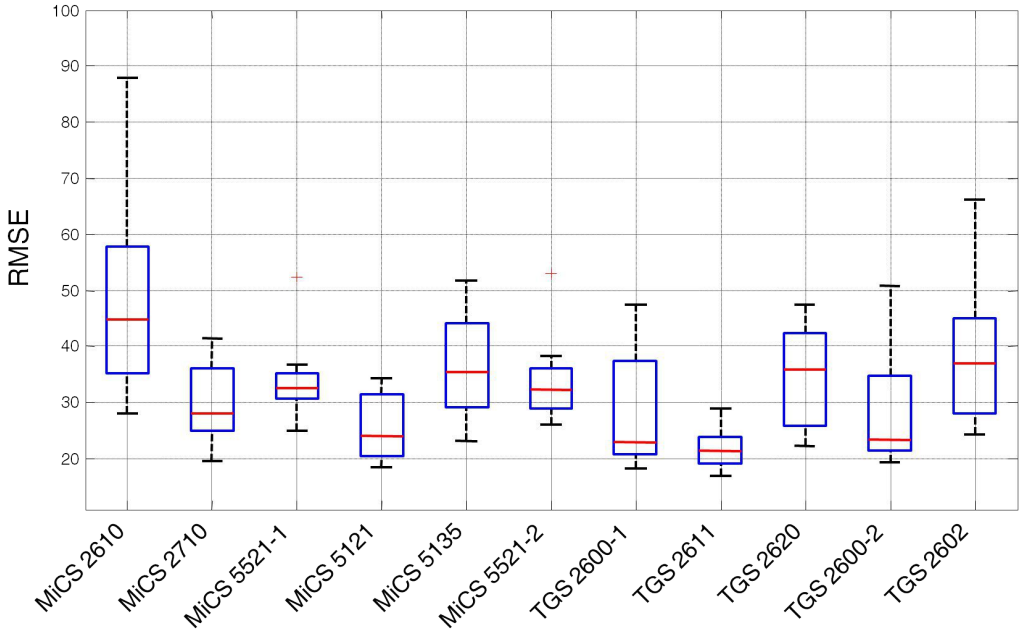

(b)

Figure 7: NLPD and RMSE box-plot for the case of one-sensor GP calibration. For both indicators, as lower the value the better the calibration. On each box, the central red mark is the median, the edges of the box are the 25th and 75th percentiles, the whiskers extend to the most extreme data points not considering outliers, and outliers are plotted individually as red crosses.

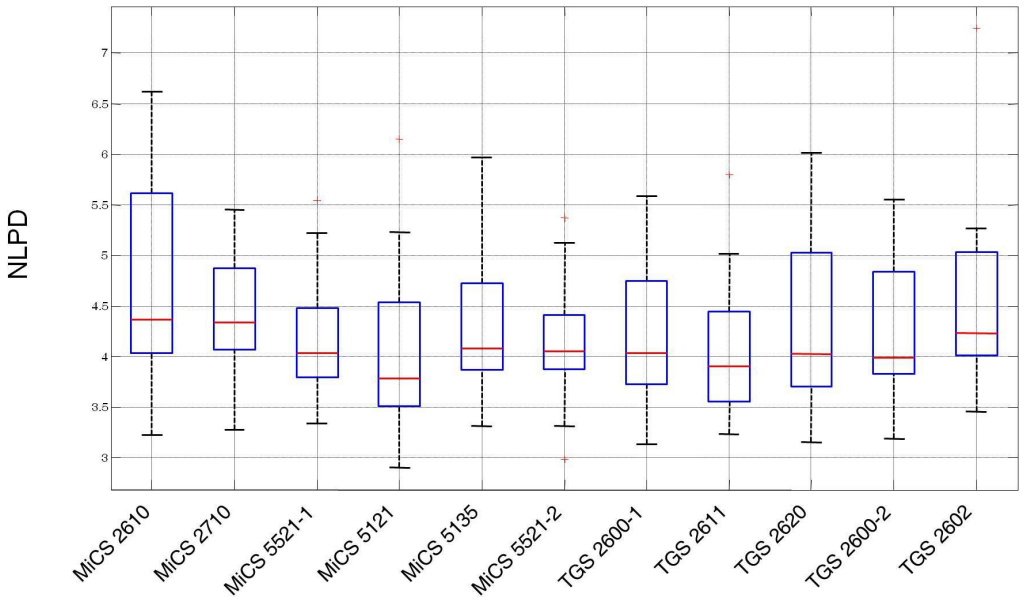

(a)

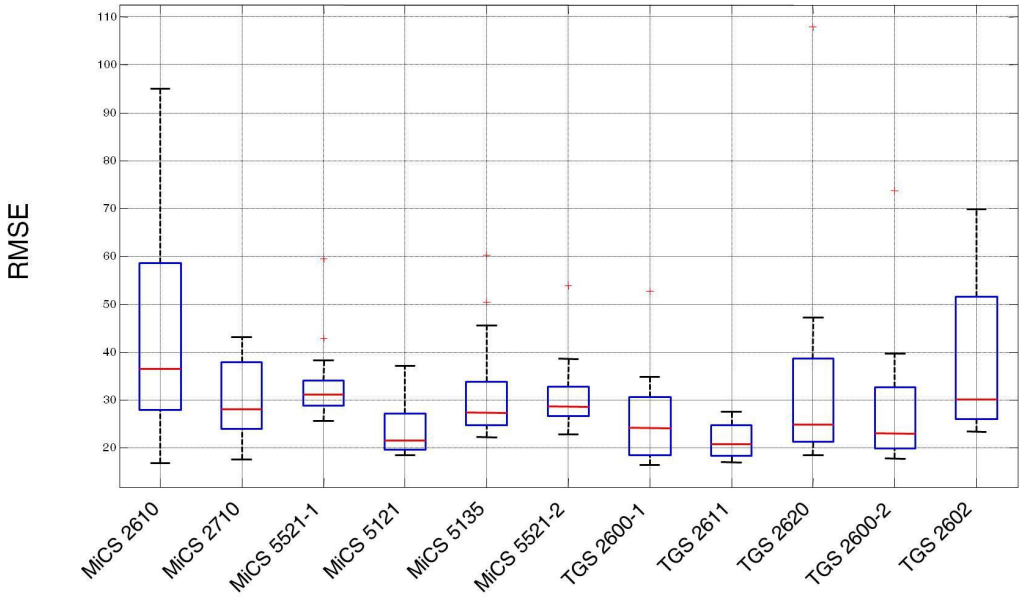

(b)

Figure 8: NLPD and RMSE box-plot for the case of one-sensor GP calibration with logarithmic transformation. For both indicators, as lower the value the better the calibration. On each box, the central red mark is the median, the edges of the box are the 25th and 75th percentiles, the whiskers extend to the most extreme data points not considering outliers, and outliers are plotted individually as red crosses.

Authors' accepted manuscript.
The final publication is available at ELSEVIER: Sensors and Actuators B: Chemical, via:
http://dx.doi.org/10.1016/j.snb.2013.06.053

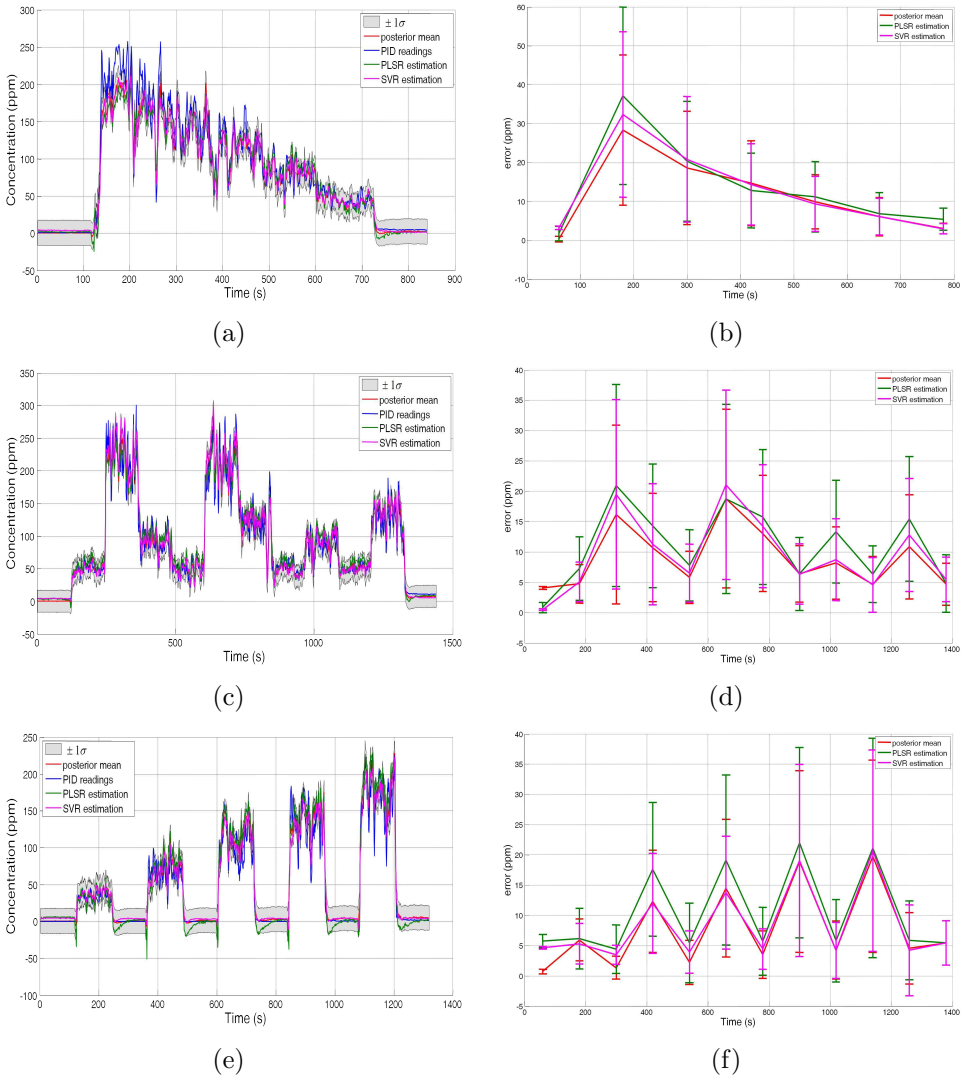

Figure 9: Estimation of the gas concentration for three different gas emitting strategies (rows) when considering the readings of the whole array and linear pre-processing $c = f(\tilde{\mathbf{r}}_\mathbf{t})$. The left column shows the ground truth (blue), together with the GP calibration estimate (the red line is the posterior mean and the shaded grey region represents the $\pm 1\sigma$ confidence interval), the PLSR (green line), and the SVR estimate (magenta line). The right column shows for each scenario the error between the different estimates and ground truth (in the case of GPs only the mean value is taken into account).

Authors' accepted manuscript.
The final publication is available at ELSEVIER: Sensors and Actuators B: Chemical, via:
http://dx.doi.org/10.1016/j.snb.2013.06.053

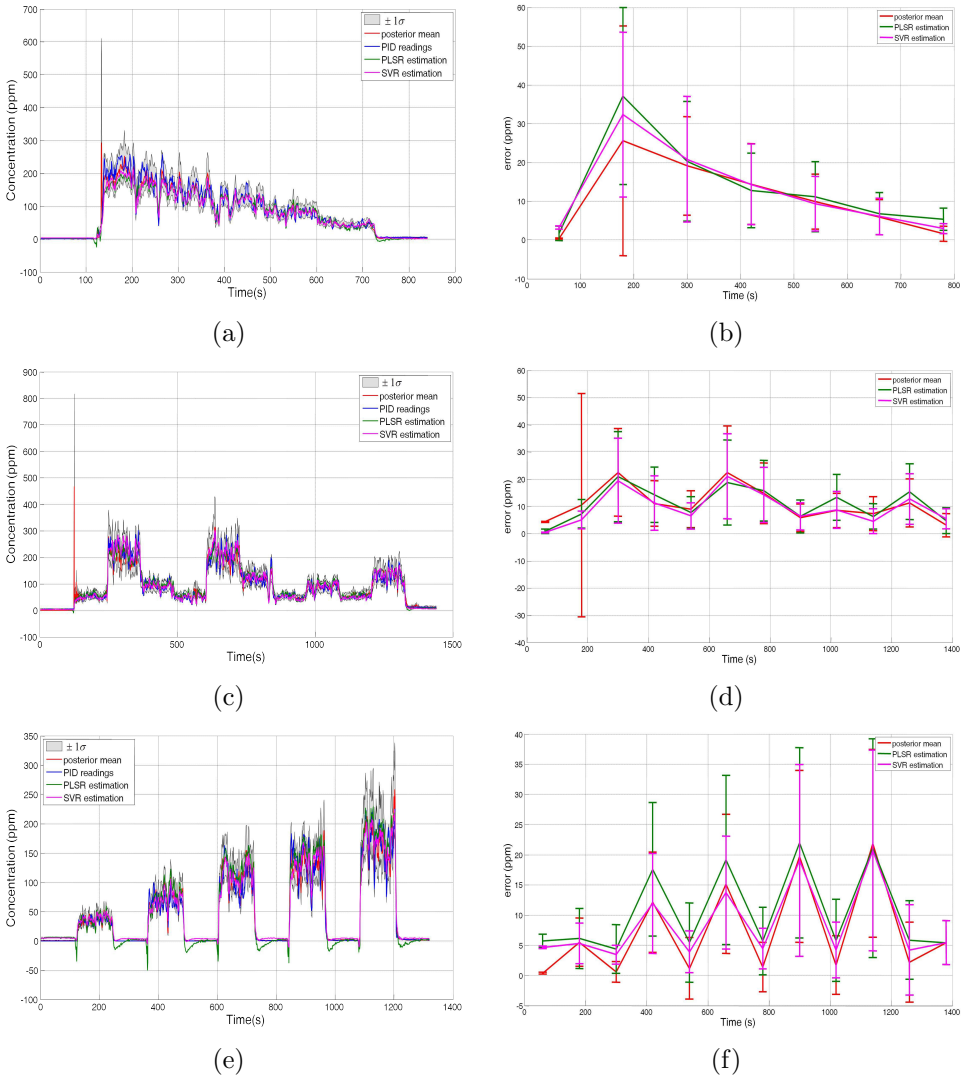

Figure 10: The predictions of the same experiment as in Figure 9, but after training with the logarithmic relation $log(c) = f(log(\mathbf{rb}(t)))$

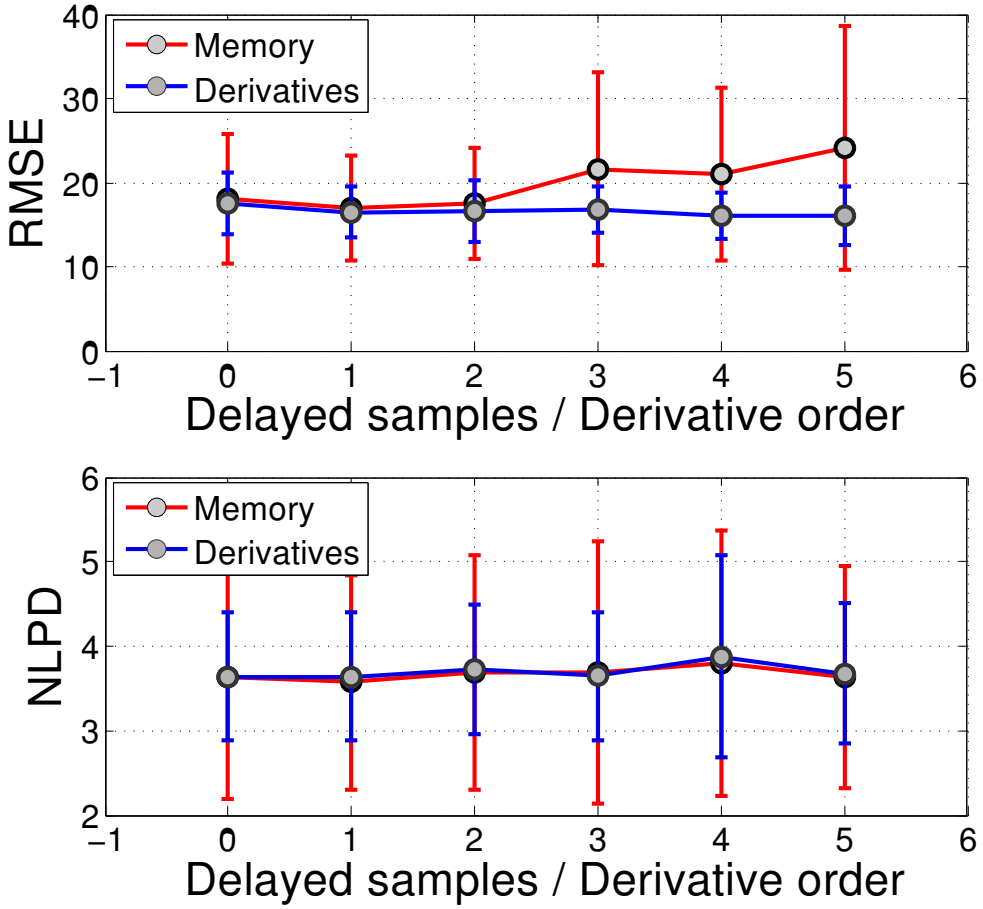

Figure 11: Mean and confidence interval ($\pm 1\sigma$) of the NLPD and RMSE of two gas concentration estimation methods, considering: (red) a number of delayed samples and (blue) derivatives with increasing order, as additional inputs.

List of Tables

Model	**Gases Detected**	**Quantity**
Figaro TGS 2600	Hydrogen, Carbon Monoxide	2
Figaro TGS 2602	Ammonia, Hydrogen Sulfide, VOC (volatile organic compound)	1
Figaro TGS 2611	Methane	1
Figaro TGS 2620	Organic Solvents	1
e2V MiCS 2610	Ozone	1
e2V MiCS 2710	Nitrogen Dioxide	1
e2V MiCS 5521	Carbon Monoxide, Hydrocarbons, VOC	2
e2V MiCS 5121	Carbon Monoxide, Hydrocarbons, VOC	1
e2V MiCS 5135	Carbon Monoxide, Hydrocarbons, VOC	1

Table 1: Gas sensors used in the sensor array.

PID	**MiCS 2610**	**MiCS 2710**	**MiCS 5521-1**	**MiCS 5121**	**MiCS 3135**	**MiCS 5521-2**	**TGS 2600-1**	**TGS 2611**	**TGS 2620**	**TGS 2600-2**	**TGS 2602**
1,00	-0,75	-0,88	-0,86	-0,89	-0,82	-0,89	-0,82	-0,92	-0,80	-0,81	-0,69
-0,75	**1,00**	0,93	0,93	0,95	0,98	0,91	0,98	0,90	0,98	0,98	0,98
-0,88	0,93	**1,00**	0,94	0,98	0,97	0,95	0,97	0,97	0,96	0,97	0,90
-0,86	0,93	0,94	**1,00**	0,98	0,97	0,99	0,96	0,97	0,96	0,96	0,90
-0,89	0,95	0,98	0,98	**1,00**	0,98	0,98	0,98	0,98	0,97	0,98	0,91
-0,82	0,98	0,97	0,97	0,98	**1,00**	0,96	1,00	0,96	1,00	1,00	0,96
-0,89	0,91	0,95	0,99	0,98	0,96	**1,00**	0,95	0,97	0,94	0,95	0,87
-0,82	0,98	0,97	0,96	0,98	1,00	0,95	**1,00**	0,95	1,00	1,00	0,97
-0,92	0,90	0,97	0,97	0,98	0,96	0,97	0,95	**1,00**	0,95	0,95	0,86
-0,80	0,98	0,96	0,96	0,97	1,00	0,94	1,00	0,95	**1,00**	1,00	0,97
-0,81	0,98	0,97	0,96	0,98	1,00	0,95	1,00	0,95	1,00	**1,00**	0,97
-0,69	0,98	0,90	0,90	0,91	0,96	0,87	0,97	0,86	0,97	0,97	**1,00**

Table 2: Cross-correlation coefficients for the MOX sensors in the array and the PID. High values suggest that the sensors are exposed to the same concentrations.

Authors' accepted manuscript.
The final publication is available at ELSEVIER: Sensors and Actuators B: Chemical, via:
http://dx.doi.org/10.1016/j.snb.2013.06.053

Sensor Model	**GPs**	**PLSR**	**SVR**
MiCS 2610	43.81 ± 22.88	44.79 ± 14.26	46.01 ± 19.44
MiCS 2710	30.38 ± 7.83	31.89 ± 6.13	29.71 ± 6.42
MiCS 5521-1	33.64 ± 9.02	34.26 ± 7.03	34.09 ± 7.56
MiCS 5121	$\mathbf{23.84 \pm 5.58}$	$\mathbf{25.44 \pm 4.20}$	$\mathbf{24.18 \pm 5.91}$
MiCS 5135	32.09 ± 12.00	35.61 ± 8.21	33.37 ± 12.31
MiCS 5521-2	31.11 ± 8.01	32.37 ± 7.47	31.80 ± 8.09
TGS 2600-1	26.05 ± 10.08	31.10 ± 5.42	25.71 ± 8.79
TGS 2611	$\mathbf{21.46 \pm 3.54}$	$\mathbf{26.27 \pm 3.59}$	$\mathbf{21.57 \pm 3.14}$
TGS 2620	34.16 ± 24.02	35.41 ± 7.08	29.61 ± 8.38
TGS 2600-2	28.96 ± 15.13	32.43 ± 5.98	27.23 ± 9.92
TGS 2602	44.64 ± 15.58	41.87 ± 8.21	37.12 ± 12.69
OVERALL	$\mathbf{31.17 \pm 6.27}$	$\mathbf{33.77 \pm 5.77}$	$\mathbf{30.94 \pm 6.78}$

Table 3: RMSE values (Mean $\pm$ 1σ) of three different calibration methods when using only one sensor at a time. Sensors *MiCS-5121* and *TGS-2611* provide the overall best performance.

Sensor	**Length scale** (l)
MiCS 2610	0.386 ± 0.272
MiCS 2710	0.732 ± 0.337
MiCS 5521-1	0.869 ± 0.145
MiCS 5121	$\mathbf{0.212 \pm 0.175}$
MiCS 5135	0.533 ± 0.312
MiCS 5521-2	0.761 ± 0.305
TGS 2600-1	0.200 ± 0.167
TGS 2611	$\mathbf{0.001 \pm 0.004}$
TGS 2620	0.554 ± 0.387
TGS 2600-2	0.749 ± 0.247
TGS 2602	$\mathbf{0.116 \pm 0.042}$

Table 4: Mean $\pm 1\sigma$ interval of the length scale hyper-parameter for the different sensors in the array as obtained from ARD.